Sandia National Laboratories is a multimission laboratory managed and operated by National Technology and Engineering Solutions of Sandia, LLC, a wholly owned subsidiary of Honeywell International, Inc., for the U.S. Department of Energy’s National Nuclear Security Administration under contract DE-NA-0003525.

Sandia National Laboratories is a multimission laboratory managed and operated by National Technology & Engineering Solutions of Sandia, LLC, a wholly owned subsidiary of Honeywell International Inc., for the U.S. Department of Energy's National Nuclear Security Administration under contract DE-NA0003525.

SAND21XX-XXXXR
LDRD PROJECT NUMBER: 21-1202
LDRD PROJECT TITLE: Pushing the Limits of High-speed X-ray Tomography to See the Unknown
PROJECT TEAM MEMBERS: Benjamin Halls (PI) (1512), Naveed Rahman (1512), Jeremy James (1515), Sam Reardon (7556), Glen White (7556), Enrico Quintana (1529), and Daniel Guildenbecher (consultant; 1512)

ABSTRACT:

First-of-their kind datasets from a high-speed X-ray tomography system were collected, and a novel numerical effort utilizing temporal information to reduce measurement uncertainty was shown. The experimental campaign used three high-speed X-ray imaging systems to collect data at 100 kHz of a scene containing high-velocity objects. The scene was a group of known objects propelled by a 12-gauge shotgun shell reaching speeds of hundreds of meters per second. These data represent a known volume where the individual components are known, with experimental uncertainties that can be used for reconstruction algorithm validation. The numerical effort used synthetic volumes in MATLAB to produce projections along known lines of sight to perform tomographic reconstructions. These projections and reconstructions were performed on a single object at two orientations, representing two timesteps, to increase the reconstruction accuracy.

INTRODUCTION AND EXECUTIVE SUMMARY OF RESULTS:

Understanding transient, three-dimensional (3D) phenomena occurring within optically opaque components is vital to many industries and applications. X-ray diagnostics are well-established and ubiquitous across many laboratories; however, state-of-the-art, high-speed X-ray tomography suffers from two severe limitations: 1) the need for quantitative high-speed 2D information, and 2) 3D tomographic techniques capable of accurately reconstructing scenes from limited views. While X-ray techniques are widespread, the current state-of-the-art is restricted to a few pulsed flash X-ray images of dynamic events, or computed tomography (CT) of static devices (requiring hundreds of views). With the recent emergence of hardware for kHz X-ray videography, high-speed X-ray CT is now feasible. However, tomography measurements have only been demonstrated up to 10-kHz imaging rates and the experiments are inherently view limited [1]. These constraints result in spatial and temporal blur, low signal-to-noise ratios, and reconstruction artifacts, all of which necessitate novel approaches to collect and extract quantitative 3D information.

The science problem is how to quantify and reduce the uncertainties of limited-view, high-speed, three-dimensional X-ray measurements to enable discovery at relevant spatial and temporal scales. Two methods to reduce this uncertainty are discussed here: developing benchmark quality

data to validate tomographic reconstruction algorithms and exploiting temporal information that is inherent to high-speed X-ray tomography experiments to reduce reconstruction uncertainty.

The state-of-the-art in CT reconstruction falls into two categories: dense CT and limited-view CT. Traditional dense CT systems provide only time- or phase-averaged data; these measurements require 100s to 1000s of views and are amenable to volume reconstruction using back-projection methods [2–5]. These methods, in brief, project the information from the images back through the volume requiring many views to achieve convergence and high spatial resolution. Iterative reconstruction techniques, however, have been developed for limited-view measurements [6–21].

For basic iterative methods, the main basis is to generate a volume that has projections that match the images along the same lines of sight, resulting in significant errors [7]. The final volume can be binarized, ensuring steep gradients, but not necessarily accurate volumes using a variety of methods [8–10]. Level-set and total variation methods, as used in computational fluid dynamics [8], have been applied to tomographic reconstruction techniques [9,10]. Therefore, blind application of current reconstruction methods could lead to false interpretation of internal component dynamics, underpinning the need for a validated reconstruction approach. The basic algorithms are available via the Livermore Tomography Toolkit (LTT) [11] and commercial software [12,13], but do not incorporate additional information about the scene. Approaches that incorporate *a priori* knowledge of the scene such as using probability distribution functions have been described in the literature [14–19]. Initialization methods have used data from the previous time step with estimated linear transformations of the volume [20]. Finally, methods to remove artifacts have been developed for iterative reconstruction techniques used in particle image velocimetry (PIV) [21]. However, each of these methods falls short in meeting the communities need for validated, accurate reconstructions.

This report addresses the questions of how to quantify and reduce uncertainty through both an experimental approach and a numerical approach, respectively. The experimental approach to quantify reconstruction uncertainty pushed a state-of-the-art X-ray tomography system in terms of spatio-temporal resolution, signal-to-noise ratios, and reconstruction uncertainties. The successful experimental campaign utilized three high-speed X-ray imaging systems, oriented every ~120˚ along the horizontal plane, to capture the flow of known objects (steel hardware) through the field of view. The objects were propelled by a short barrel 12-gauge shotgun that was placed above the field of view and fired vertically downwards. The shotgun shells were loaded with various pieces of stainless-steel hardware of know shape and quantity. Data was collected at 100 kHz and represents (to the best of the authors knowledge) both the fastest limited-view X-ray tomography at this scale, and a measurement of known objects that can be used to quantify the accuracy of reconstructions of dynamic scenes with true experimental uncertainties. These long-sought data can now be used to quantify current and future methods of tomographic reconstruction and camera calibration / registration procedures. The numerical approach applied a method to use temporal information that reduced reconstruction uncertainties using synthetic tomography. The synthetic tomography system, built in MATLAB, creates a known volume, generates projections of the

volume, and then uses the projections to perform the tomographic reconstruction. This method was used to compare two reconstructions of a single object that was undergoing simulated rigid body motion, therefore in a different orientation and imaged from two different sets of three views relative to the object. It was found that the reconstructions for each orientation had similarities and differences, and that use of the information from both resulted in a more accurate reconstruction.

DETAILED DESCRIPTION OF RESEARCH AND DEVELOPMENT AND METHODOLOGY:

Benchmark Experiment Campaign

The experiments to benchmark reconstruction algorithms have three main requirements: they needed to be dynamic, have realistic measurements uncertainties, and they needed to have a known solution such that the volume reconstructions can be compared to something to quantify the uncertainty. To meet both needs, an experiment with a high velocity flow using known objects in the field provides a method of determining the ground truth. The scene chosen to be imaged was stainless steel hardware fired from a remotely operated 12-gauge shotgun. The shape, mass, and quantity of the objects was predetermined for each shot. The short-barrel shotgun was fired downwards into a catchment containing ground rubber to safely decelerate and collect the high-velocity objects. The objects were imaged by three high-speed X-ray imaging systems placed horizontally around the field of view each spread out by 120˚, shown in Fig. 1. Shows a photograph and a schematic of the experimental setup.

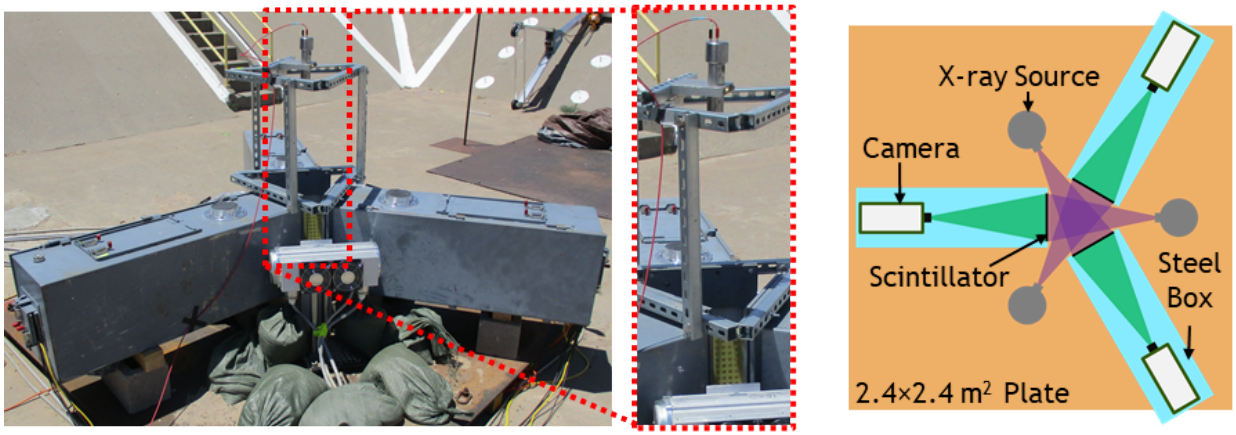

Figure 1. Photograph of the experimental setup, including the shotgun supported by the metal structure (left), and a schematic of the three X-ray imaging systems (right) positioned at angles 0, 120, and 240˚ about the horizontal axis.

The source to scintillator distance was 60 cm and the geometric magnification was ~1.5. The X-ray sources were Varian G-297 rotating anode sources operated at 145 kV and 500 mA with 6 mm polycarbonate shielding. The scintillators were made by Scinticor and had 7 μs decay time. The cameras were Phantom 2512s and had Zeiss 25 mm f/1.4 objectives. The cameras and

scintillators were enclosed in steel boxes with 6 mm thick polycarbonate shields in front of the scintillators and 1 mm equivalent lead glass in front of the cameras.

During the tests, each imaging system was synchronized and ran at a repetition rate of 100 kHz and collected images of both the objects passing through the field of view, and before the objects arrived for flat field corrections. Prior to the tests, three sets of calibration images were collected for 1) camera registration, 2) to determine the spectral response of the system, and 3) to account for dark signals (intensity on the camera chip not caused by the opposing X-ray source). Images of a dot calibration board at several locations were collected to enable camera registration for tomographic reconstruction. The X-ray spectral response of the imaging system was determined by imaging various known thicknesses of stainless steel. This calibration accounted for the non-linear transmission of polychromatic X-rays as well as the scintillator response function. Lastly the dark signals for each camera were collected separately by running the two adjacent X-ray sources. These images contained all the signal except that coming from the opposed / intended X-ray source. These signals account for the background that is subtracted from the images prior to flat-field normalization during image processing.

The image processing involved subtraction of the dark signals, normalization by the flatfield images collected before the objects entered the field of view, and conversion from normalized transmission images to path length using the spectral calibration. Flatfield images and spectral calibration images were dark signal subtracted and both dark signal and flat-field normalized, respectively. The dot calibration images are flat-field normalized to aid the algorithm in locating the dots. These data are then ready to be used by any number of reconstruction algorithms to help determine the reconstruction accuracy.

The iterative reconstruction process consists of two steps: camera registration and volume reconstruction. The camera registration locates the dots relative to themselves and also to the other cameras to determine the camera parameters and a common coordinate system. Next, the images are fed into the reconstruction script where a Multiplied Line Of Sight (MLOS) algorithm is used to initialize the reconstructed volume. From there an iterative process of comparing the experimental images to projections of the volume along the same lines of sight was utilized. A Maximum-Likelihood Expectation-Maximization (MLEM) algorithm is used to adjust the reconstructed volume to minimize the differences between the experimental images and volume projections. Once a threshold is met the reconstruction process is complete.

Numerical Study of Temporal Information

The numerical study to test the feasibility of using temporal information to increase reconstruction accuracy was tested using synthetic data in MATLAB. For this study a volume of a single flat ring was created and rotated about its center of mass to represent what the object would look like if it were tumbling through the field of view. This volume represents the ground truth from which projections can be generated. Figure 2 shows an isosurface of the ring and projections along the major axis (normal to the ring) and minor axis (parallel to the ring). The projections were integrations of the volume along the lines of sight, representing a perfect parallel beam image of

the ring. Using a parallel beam approximation is not unreasonable for small objects and reduces the computational expense during projection generation and volume reconstruction.

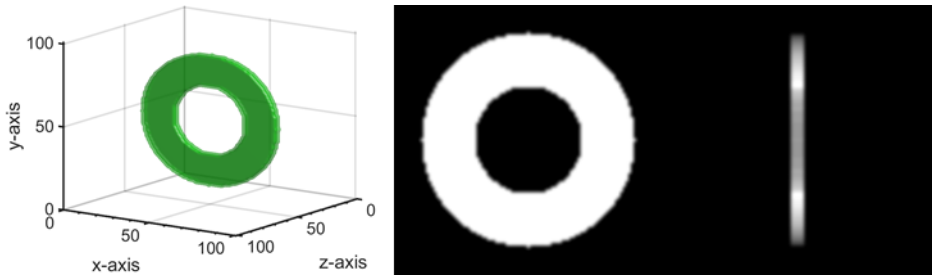

Figure 2. Known ring object (left), and linear projections (right) along the major axis and minor axis of the ring.

The contrast of the projections in Fig. 2 and all of the following figures containing projections have been stretched to show the most detail. The projections of the volume did not require any processing because they were linear summation rather than a synthetic radiograph. This method was chosen to keep experimental uncertainties to a minimum thereby isolating and placing focus on the reconstruction uncertainties. The reconstruction process was as described above, MLOS initialized, followed by an MLEM algorithm.

RESULTS AND DISCUSSION:

Benchmark Experiment Campaign

A sample of the normalized images from the benchmark experiment campaign are show in Fig. 3. The dark objects in the image are the pieces of stainless-steel hardware and the grey object in the image above the hardware is the plastic wadding from the shot gun shell.

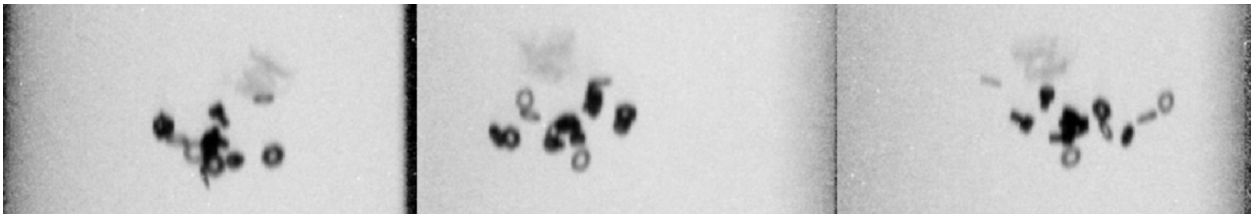

Figure 3. Normalized radiographs of the objects at approximate angles of 0, 120, and 240˚ about the vertical axis.

These images were converted to path length images using the calibration and are shown in Fig. 4. Either the transmission images or the pathlength images can be used for tomographic reconstruction. The conversion from transmission to path length can be done prior to or within the algorithm. Since all the objects are of the same material it is easier to perform the conversion prior to running the algorithm to reduce the computational expense.

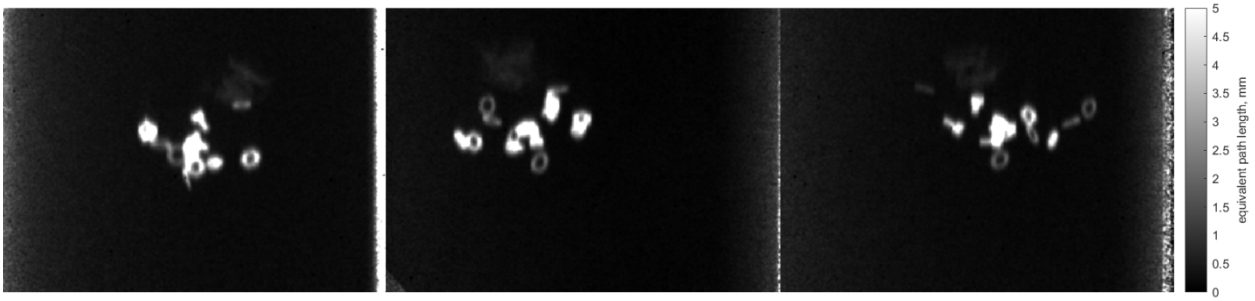

Figure 4. Path length images of the objects at approximate angles of 0, 120, and 240˚ about the vertical axis.

For these experiments the path length images were used during the reconstruction process. The reconstructed volume is shown in Fig. 5. Due to the inherent under-resolved nature of limited-view tomography, the reconstructed volume represents one of many solutions that can satisfy the requirement of the volume projections matching the experimental images. Therefore, it is necessary to compare various algorithms against benchmark data with realistic experimental uncertainties to understand which algorithms may produce the best reconstructions.

Numerical Study of Temporal Information

The numerical study produced synthetic volumes of the ring at two different orientations. The first orientation, shown in Fig. 5, has the major axis placed along the *xy* plane. The second orientation, shown in Fig. 7, has the major axis placed along *xz* plane. The large difference in orientation was chosen to maximize the difference in the reconstructions and highlight the accuracies and inaccuracies representing a best-case scenario for using a temporal method such as shown.

Figure 5. Isocontours of the ring volume orientation 1 (left), and linear projections at 0, 120, and 240˚ (right).

The projections of the ring in Fig. 5 are quite favorable for defining the outer regions of the ring, particularly along the major axis. These projections and known angles were fed into the reconstruction algorithm and the results are shown in Fig. 6.

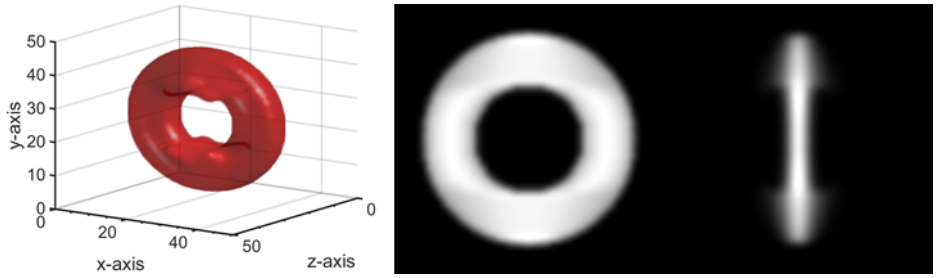

Figure 6. Isocontours of the reconstructed volume (left), and the projections along the major and minor axes (right).

The volume reconstructed from the projections in Fig. 5 is a single realization of a volume that satisfies the image–projection difference minimization. As previously discussed, the reconstruction for this orientation does a good job estimating the ring along the major axis.

Figure 7. Isocontours of the ring volume orientation 2 (left), and linear projections at 0, 120, and 240˚ (right).

The projections of the ring in Fig. 7 are favorable for defining the regions of the ring along the minor axis. These projections and known angles were fed into the reconstruction algorithm and the results are shown in Fig. 8.

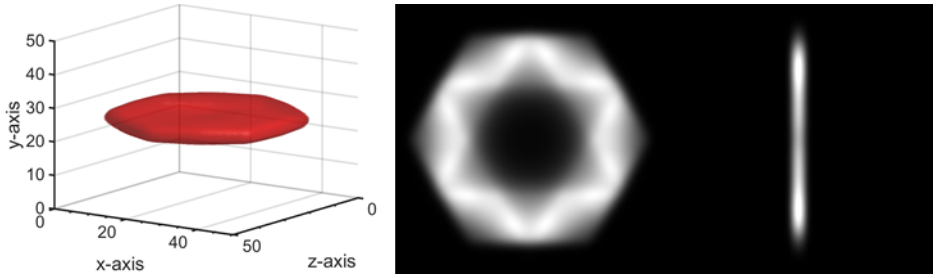

Figure 8. Isocontours of the reconstructed volume (left), and the projections along the major and minor axes (right).

The volume reconstructed from the projections in Fig. 7 is again a single realization of a volume that satisfies the image–projection difference minimization. As previously discussed, the reconstruction for this orientation does a good job estimating the ring along the minor axis. As seen in both reconstructions the orientation of the angles plays a large role on the shape and accuracy of the reconstruction. For one orientation the major axis compares well, and the minor

axis compares poorly, and the opposite is true for the other orientation. Therefore, it is necessary to use information from both orientations (time steps as it would be in an experiment) to see if the reconstructions can be enhanced.

A straightforward and computationally low-cost method to use information from both volumes was chosen. The square root of the product of the reconstructions was used, where it is assumed the most-true information will overlap, and maintain a similar integrated intensity. The challenge then is to ensure the orientations of the reconstructions are matched prior to taking the product. To accomplish this the angular difference in the two reconstructions was determined by the cross-correlation of the volumes while rotating the reconstruction from orientation two about its center of mass. While the angle between the orientations was predetermined the simple algorithm was used to show the feasibility of the technique when the values are unknown. Here the center of mass would be the center of the volume for both orientations which is simple, and in the case of an experiment the center of mass is readily calculated given the quantitative nature of the processed path length images. Figure 9 shows the volumes that are being rotationally corelated to find the most likely angle used to calculate the new volume. The process goes through a course scan (every 10 degrees) followed by a fine scan (every 1 degree). In the case of experimental data, the correlation would be two dimensional since neither angle would be known.

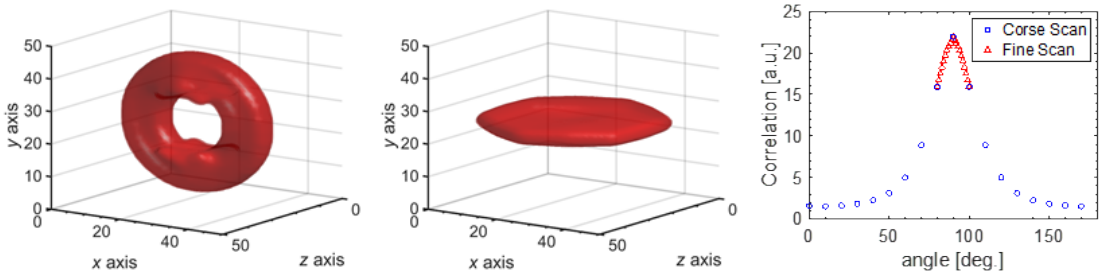

Figure 9. Isocontours of the two volumes one stationary (left) and one being rotated to find the correlation (middle), and the plot of correlation value as a function of angular rotation (right).

Shown in Fig. 10, the final reconstruction now has a favorable shape along both the major and minor axes. This method, with a small computation expense relative to the initial reconstructions themselves, serves as one path forward for using temporal information to reduce the uncertainty in limited-view tomographic reconstruction.

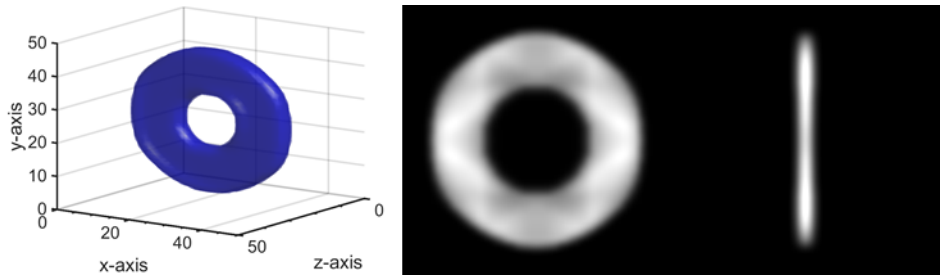

Figure 10. Isocontours of the square root of the product of both reconstructions in Figs. volume (left), and the projections along the major and minor axes (right).

ANTICIPATED OUTCOMES AND IMPACTS:

These data are not only novel in that they have a known solution to compare the volume reconstruction against and define reconstruction accuracy, but they are also a ten-fold increase in temporal resolution over previously published results [1]. The goal is to have the results available to the research community such that they can use the experimental results to validate various open-source algorithms or algorithms that they have developed themselves. This work is unique in that X-ray tomography systems using quasi-CW are becoming more and more popular and therefore there is a lot more information within the data that can utilized to reconstruct the scene with greater accuracy. The use of temporal information, as shown here, represents one of several methodologies to increase the reconstruction accuracy with information already known about the scene. The cost and experimental limitations of only a few views will likely hold true for many applications, therefore the reconstruction algorithm is a great pathway to reduced uncertainty.

The next steps of this work are to continue and expand the development of benchmark quality data and reconstruction advancements. The benchmark data will include more experimental efforts of highly dynamic scenes, experimental efforts using more views to reconstruct the motion of components and simple systems, as well as developing synthetic tomographic reconstruction methods where the datasets can utilize known geometries or data directly from computational methods. The experimental efforts bring the true measurement uncertainties to the forefront, whereas the synthetic datasets have unlimited flexibility in what is to be reconstructed, from how many views, and various amounts of image noise, spatial and temporal blur. The long-term goal is to couple the reconstruction advancements and the benchmark data into a single package for four-dimensional measurements with reconstruction uncertainty quantification.

The impact of this work is the development of a validated, advanced reconstruction algorithm that can be used across the Labs for on-going and future measurement campaigns. The ability to accurately reconstruct a three-dimensional scene from a limited number of views is an open problem among researchers. While there are past and current efforts to increase the reconstruction accuracy, they are not all validated nor are they accessible though as single piece of software. Additionally, determining the actual uncertainties of a reconstruction are very difficult to define. With bounded uncertainties, the confidence in the experimental data will drive the need and applicability of the knowledge gain from such experiments. Such a validated algorithm will enable novel research of harsh three-dimensional environments.

CONCLUSION:

Benchmark experiments were conducted to obtain experimental results from a known volume that can help define tomographic reconstruction accuracy and validate a wide range of algorithms and techniques. The dynamic images with calibration data and camera registration

images can be made available for use by the community at large. The numerical study has shown a straightforward, computationally inexpensive method to utilize temporal information to increase the accuracy of limited-view tomography experiments. Both of these efforts represent initial studies that can evolve to larger studies to continue the development of limited-view tomography.

REFERENCES:

1. Halls, B.R., N. Rahman, M.N. Slipchenko, J.W. James, A. McMaster, M.D.A. Ligthfoot, J.R. Gord and T.R. Meyer (2019), 4D spatiotemporal evolution of liquid spray using kilohertz-rate x-ray computed tomography, Opt. Lett., 44(20), doi:10.1364/OL.44.005013.
2. Feldkamp, L.A., L.C. Davis and J.W. Kress (1984), Practical cone-beam algorithm, J. Opt. Soc. Am. A, 1, doi:10.1364/JOSAA.1.000612.
3. Kak, A.C. and M. Slaney (1988), Computerized Tomographic Imaging, IEEE Press, New York.
4. Jimenez, E.S. and L.J. Orr (2013), Rethinking the union of computed tomography reconstruction and GPGPU computing, Proc. 8854, Penetrating Radiation Systems and Applications XIV; 88540A, doi:10.1117/12.2029995.
5. Jimenez, E.S., L.J. Orr and K.R. Thompson (2012), An Irregular Approach to Large-Scale Computed Tomography on Multiple Graphics Processors Improves Voxel Processing Throughput, 2012 SC Companion: High Performance Computing, Networking Storage and Analysis, doi:10.1109/SC.Companion.2012.42.
6. Beister, M., D. Kolditz, W.A. Kalender (2012), Iterative reconstruction methods in X-ray CT, Phys. Medica, 28(2), doi:10.1016/j.ejmp.2012.01.003.
7. Schmidlin, P., M.E. Bellemann and G. Brix (1999), Subsets and overrelaxation in iterative image reconstruction, Phys. Med. Biol., 44(5), doi:10.1088/0031-9155/44/5/321.
8. Arienti, M. and M. Sussman (2014), An embedded level set method for sharp-interface multiphase simulations of Diesel injectors, Int. J. Multiph. Flow, 59, doi:10.1016/j.ijmultiphaseflow.2013.10.005.
9. Estellers, Virginia & Zosso, Dominique & Lai, Rongjie & Osher, Stanley & Thiran, Jean-Philippe & Bresson, Xavier (2012), An Efficient Algorithm for Level Set Method Preserving Distance Function, IEEE transactions on image processing: a publication of the IEEE Signal Processing Society, 21, doi:10.1109/TIP.2012.2202674.
10. Demircan-Tureyen, E. and M.E. Kamasak (2017), A discretized tomographic image reconstruction based upon total variation regularization, Biomed. Signal Proces., 38, doi:10.1016/j.bspc.2017.03.015.
11. Champley, K. (2016), Livermore Tomography Tools (LTT) Technical Manual, LLNL-SM-687016.
12. Hansen, P.C. and M. Saxild-Hansen (2011), A MATLAB package of algebraic iterative reconstruction methods, J. Comput. Appl. Math., 236, doi:10.1016/j.cam.2011.09.039.
13. Gürsoy, D., F. De Carlo, X. Xiao and C. Jacobsen (2014), Tomopy: a framework for the analysis of synchrotron tomographic data, J. Synchrotron Radiat., 21(5), doi:10.1107/S1600577514013939.

14. Hanson, K.M. and G.W. Wecksung (1983), Bayesian approach to limited-angle reconstruction in computed tomography, J. Opt. Soc. Am., 73(11), doi:10.1364/JOSA.73.001501.
15. Grauer, S.J., P.J. Hadwin and K.J. Daun (2016), Bayesian approach to the design of chemical species tomography experiments, Appl. Opt., 55(21), doi:10.1364/AO.55.005772.
16. Daun, K.J., S.J. Grauer, and P.J. Hadwin (2016), Chemical species tomography of turbulent flows: discrete ill-posed and rank deficient problems and the use of prior information, J Quant. Spectrosc. RA 172, doi:10.1016/j.jqsrt.2015.09.011.
17. Minerbo, G. (1979), Maximum entropy reconstruction from cone-beam projection data, Comput. Biol. Med., 9(1), doi:10.1016/0010-4825(79)90020-9.
18. Gull, S.F. and T.J. Newton (1986), Maximum entropy tomography, Appl. Opt., 25(1), doi:10.1364/AO.25.000156.
19. Smith, R.T., C.K. Zoltani, G.J. Klem and M.W. Coleman (1991), Reconstruction of tomographic images from sparse data sets by a new finite element maximum entropy approach, Appl. Opt., 30(5), doi:10.1364/AO.30.000573.
20. Lynch, K.P. and F. Scarano (2015), An efficient and accurate approach to MTE-MART for time-resolved tomographic PIV, Exp. Fluids, 56(66), doi:10.1007/s00348-015-1934-6.
21. Scarano, F. (2013), Tomographic PIV: principles and practice, Meas. Sci. Tech., 24(1), doi:10.1088/0957-0233/24/1/012001.